Capacity bounds of Low-Dense NOMA over Rayleigh fading channels without CSI

Mai T. P. Le*‡, Giuseppe Caso*, Luca De Nardis*, Alireza Mohammadpour*, Gabriele Tucciarone*
and Maria-Gabriella Di Benedetto*
*Department of Information Engineering, Electronics and Telecommunications,
Sapienza University of Rome, Rome 00184, Italy
‡ Email: mai.le.it@ieee.org

***Abstract*—Upper and lower bounds on capacity of low-dense code-domain NOMA were investigated in the context of 5G New Radio (5G-NR), under the worst hypothesis of no channel knowledge at the receiver, i.e. operation without channel state information (CSI). The impact of peculiar features of 5G-NR on capacity bounds of optimum receivers was investigated. The upper bound, defined as the system capacity with perfect CSI, and the lower bound corresponding to a pilot-based communication model, were found. These bounds indicated that the achievable rates of low-dense code-domain NOMA without CSI are lower, as expected, than those with perfect CSI, although the above gap vanishes to negligible values, when some of the system parameters, in particular speed of variation of the channel against symbol duration, number of simultaneous users, and system load, i.e. number of users vs. number of resource elements, favorably combine.**

***Index Terms*—code-domain NOMA, pilot-based communication, low-dense, non-coherent capacity.**

I. Introduction

In recent real-world mobile communication channels, the rapid change of fading coefficients may severely affect estimation at the receiver. Receivers may have, in fact, no knowledge of channel state information (CSI), i.e. channel state information at the receiver (CSIR), except for the distribution of channel gains, a condition that is commonly referred to as *noncoherent setting* [1]. As a consequence, capacity, i.e. the fundamental criterion for predicting achievable rates, may be reduced compared to ideal conditions of perfect CSI detection, leading to a so-called noncoherent capacity [1], [2].

Code-domain non-orthogonal multiple access (NOMA) is a potential candidate for multiple access in 5G, thanks to its high spectral efficiency and possibility of offering massive connectivity, and robust connection in very high mobility scenarios [3], [4]. As a matter of fact, NOMA is a study item for 5G-New Radio (5G-NR), the standardization of which was launched by 3GPP in April 2016, with two phases aimed at defining 5G specifications before its commercialization in 2020. While other 5G specifications are ongoing, the parameters of the radio framework were already specified in the very recent 3GPP specification TS 38.211 [5]. Understanding channel capacity for code-domain NOMA system in the absence of CSIR becomes, hence, essential. Closed-form expressions for noncoherent capacity are, however, difficult to obtain, even for the 'easy' memoryless channel [1], leading to a common practice to look for upper and lower capacity bounds, where the upper bound naturally corresponds to the capacity with perfect CSIR (coherent capacity) [6]. In order to find the lower bound, a popular method is to adopt a pilot-based communication model, for example, for the continuous fading model [7], and for the block-fading model [8].

This paper investigates capacity bounds of low-dense code-domain NOMA over Rayleigh fading channels without CSIR, based on the framework presented in [4]. The upper bound can be readily evaluated via the corresponding coherent capacity [4], whereas the lower bound can be derived via the capacity of a pilot-based communication scheme.

The paper is organized as follows. Section II describes the channel and signal models. Capacity bounds are presented in Sec. III. Results and discussion are reported in Sec. IV. Section V concludes the paper.

II. System model

A. Channel model: Rayleigh block-fading assumptions

To reflect the nature of fading communication, either continuous or block-fading model can be selected to derive the capacity bounds with the duality property [8], [9]:

$$n_b = \frac{1}{2 f_m T_s}, \tag{1}$$

where n_b represents the number of coherent symbols within a block in which the channel is considered stationary (block-fading model), T_s is the symbol period, $f_m = v f_c / c$ is the maximum Doppler frequency, f_c being the carrier frequency, v is the velocity of interest, and c is the speed of light. n_b can be considered as the discretized version of the coherence time T of a continuous-fading model. For 3GPP LTE and IEEE 802.16 WiMAX, the values of n_b may range from unity to several hundreds [8], or even to thousands for 5G-NR as further detailed in Section IV.

B. Signal model

The model provided in [4] for low-dense code-domain NOMA was adopted, with the inclusion of a Rayleigh block-fading model. The channel model is rewritten as

$$\boldsymbol{Y} = \boldsymbol{SAX} + \boldsymbol{N}, \tag{2}$$

where $\boldsymbol{Y} \in \mathbb{C}^{N\times n_b}$ is the received signal with N referring to the number of resource elements (REs); $\boldsymbol{X} = [\boldsymbol{x}_1, \ldots, \boldsymbol{x}_K]^{\mathsf{T}} \in \mathbb{C}^{K\times n_b}$ with $\boldsymbol{x}_k$ being the row-vector including n_b symbols transmitted by the k-th user; $\boldsymbol{S} = [\boldsymbol{s}_1, \ldots, \boldsymbol{s}_K] \in \mathbb{R}^{N\times K}$ is a random spreading matrix, column k being the unit-norm spreading sequence of user k; $\boldsymbol{A} \in \mathbb{C}^{K\times K}$ is a diagonal matrix of complex-valued fading coefficients $\{a_1, \ldots, a_K\}$; and $\boldsymbol{N} \in \mathbb{C}^{N\times n_b}$ denotes the noise with each column-vector $\boldsymbol{n} \in \mathbb{C}^N$ being described by a circularly-symmetric Gaussian random vector with zero mean and covariance matrix $\mathcal{N}_0\boldsymbol{I}$. Compared to [4], vectors $\boldsymbol{y}$, $\boldsymbol{n}$, $\boldsymbol{x}$ are expanded with an additional dimension, since the reference unit is now a coherence block consisting of n_b symbols rather than one symbol, whereas matrices $\boldsymbol{A}$ and $\boldsymbol{S}$ still hold in the new context.

The massive connectivity feature of 5G networks, that is, the large number of users that the system must provide with robust access simultaneously, is well reflected in a typical *asymptotic* analysis, where both the number of users K and the REs N go to infinity, while *system load* $\beta = K/N$ is kept constant, known as system analysis in the asymptotic regime. As a matter of fact, the fundamental limits of code-domain NOMA and traditional DS-CDMA frameworks in the asymptotic regime were provided in [4] and [10] as further detailed in Section III.

Noteworthy that the channel model in eq. (2) is equivalent to the general model $\boldsymbol{Y} = \boldsymbol{H}\boldsymbol{X} + \boldsymbol{N}$ given in [11] for DS-CDMA, where $\boldsymbol{H} \in \mathbb{C}^{N\times K}$ is replaced by $\boldsymbol{S}\boldsymbol{A} \in \mathbb{C}^{N\times K}$. As stated by Tulino and Verdú in [11], the dimension roles of N and K of matrix $\boldsymbol{H}$ may assume different meanings for different systems; N and K are, for instance, the number of users vs. chips (REs) in DS-CDMA [10] and time-hopping CDMA [12], or the number of receiving (n_R) and transmitting (n_T) antennas in multiple-input multiple-output (MIMO). Therefore, results obtained for the different systems can be reused provided that a same signaling model holds, and the parameters are given the right meaning. In particular, the capacity lower bound for code-domain NOMA can be derived based on the analysis of lower bound for a MIMO system, provided by a pilot-based scheme [7].

III. Capacity bounds of low-dense code-domain NOMA

In this section, we find the optimum capacity bounds of low-dense code-domain NOMA in the noncoherent setting with the upper bound given by the capacity with perfect CSIR (coherent capacity) [4] and the lower bound based on the capacity of a pilot-based scheme originally proposed by Hassibi and Hochwald [7], and further refined by Rusek *et al.* [8].

A. Capacity upper bound

The ergodic capacity with perfect knowledge of the channel at the optimum receiver provided for the general model when $\boldsymbol{X}$ is a circularly-symmetric complex Gaussian with zero mean and covariance $\boldsymbol{Q}$, in bits/s/Hz, is provided in [13], and writes:

$$C = \mathbb{E}\left[\log_2 \det\left(\boldsymbol{I}_N + \boldsymbol{H}\boldsymbol{Q}\boldsymbol{H}^*\right)\right], \tag{3}$$

where $\boldsymbol{I}_N$ denotes the identity matrix.

For code-domain NOMA, eq. (3) becomes [4]:

$$C(\mathrm{SNR}) = \mathbb{E}\left[\log_2 \det\left(\boldsymbol{I}_N + \mathrm{SNR}\boldsymbol{S}\boldsymbol{A}\boldsymbol{A}^*\boldsymbol{S}^*\right)\right], \tag{4}$$

whereas for single-user MIMO [11], the capacity is

$$C(\mathrm{SNR}) = \mathbb{E}\left[\log_2 \det\left(\boldsymbol{I}_N + \frac{\mathrm{SNR}}{K}\boldsymbol{H}\boldsymbol{H}^*\right)\right]. \tag{5}$$

The presence of coefficient $1/K$ in eq. (5) may be explained based on the fact that the transmitted power is divided equally among K transmitting antennas, while in the NOMA model, each user transmits with full power (see eq. (4)).

The closed-form expression of coherent capacity for the particular case of low-dense code-domain NOMA in the asymptotic regime is as follows [4]:

$$C(\beta, \mathrm{SNR}) = \sum_{k\geqslant 1} \frac{e^{-\beta}\beta^k}{k!} \int_0^\infty \frac{e^{-\lambda}\lambda^{k-1}}{(k-1)!} \log_2(1 + \mathrm{SNR}\lambda)\, d\lambda, \tag{6}$$

where β is the system load, and the first term of right-hand side expression of eq. (6) is the probability density function (PDF) of a compound Poisson distribution with exponentially-distributed summands.

B. Capacity lower bound

In this section, capacity lower bound for low-dense NOMA is derived from the capacity of a pilot-based communication [7], [8]. First, a description of the pilot-based is provided, then, a follow-up discussion on optimizing the number of pilot symbols is presented, and two capacity lower bounds of low-dense NOMA corresponding to two different ways of allocating power to the pilots conclude the section.

1) Pilot-based channel model: Two phases typically characterize a pilot-based scheme: the pilot phase and the data transmission phase, where the latter is implemented after a minimum mean-square error (MMSE) channel estimation obtained during the pilot phase. Among the total n_b symbols of a fading block, n_p symbols, called pilot symbols, are allocated for learning the channel, and the remaining $(n_b - n_p)$ are dedicated for data transmission.

Three assumptions rule the pilot-based scheme proposed in this work. First, based on 5G properties as will be also indicated in Section IV, n_b is much greater than both $\{K, N\}$, and it is, therefore, reasonable to assume $n_b > 2K$, i.e. the number of users is always lower than half the number of coherence symbols. Secondly, perfect channel estimation (via pilot phase) is assumed. Lastly, each transmission is assumed to be self-contained, that is, both pilot and data phases are referred to a specific fading block of n_b symbols [8]; specific iteration of the procedure including training, estimation and data transmission is applied to each block.

Pilot phase : For pilot symbols, one can write:

$$\boldsymbol{Y}_p = \boldsymbol{S}\boldsymbol{A}\boldsymbol{P} + \boldsymbol{N}_p, \tag{7}$$

where $\boldsymbol{P} \in \mathbb{C}^{K\times n_p}$ is the matrix of known pilot symbols replacing the transmitted signal $\boldsymbol{X}$ with the constraint $\boldsymbol{P}\boldsymbol{P}^* = n_p\boldsymbol{I}$, $\boldsymbol{Y}_p$ and $\boldsymbol{N}_p$ are matrices of size $N \times n_p$.

Data transmission phase : In this phase, a similar equation to eq. (2) can be applied with new dimensions of output and input being $N \times (n_b - n_p)$ and $K \times (n_b - n_p)$, respectively.

2) Optimizing the number of pilot symbols: The number of pilot symbols n_p directly affects the fundamental limits of a system in the noncoherent setting, and the issue of defining the optimal n_p has been extensively investigated in the literature [2], [7], [8]. If n_p is too small, the time dedicated to channel sounding may be insufficient to provide good estimates, while a too large n_p value implies reduced data transmission rates [7].

An early study on the multi-antenna channel capacity by Marzetta [14], showed that to optimize the throughput of a pilot-based scheme, one should, in general, spend half of coherence time for training. The later work on multi-antenna capacity by Hassibi and Hochwald [7] provided a fine description of the optimal training interval as a function of the number of transmitting antennas K, receiving antennas N, fading coherence time T, and SNR. In fact, it was shown that in case of either low SNR or T slightly larger than K, the pilot-based scheme is suboptimal; oppositely, when SNR is high or $T \gg K$, the lower bound capacity provided based on the pilot scheme approaches the coherent capacity. As detailed in Section IV, for code-domain NOMA with pilot-based channel estimation, capacity bounds can be analyzed under the impact of the number of symbols within a coherence block n_b, the number of users K, and the number of REs N (via the system load $\beta = K/N$).

3) The effect of pilot power allocation: Another condition also directly affecting capacity of pilot-based systems is pilot power allocation. In general, in order to have tight capacity bounds, a favorable condition is to avoid imposing constraints on power allocated to pilot symbols. Two capacity lower bounds are derived below, with no power constraint vs. with constraint.

a) No constraint on pilot power allocation: If one can freely allocate power to pilot and data symbols (*pilot power-boosting* mode), the optimum number of pilot symbols is equal to the number of users, that is, $n_p = K$ [2], [7]. Intuitively, to learn the channel properly, the receiver should receive at least one pilot symbol from each user, i.e. K pilot symbols in total. The lower bound of nonherent capacity of code-domain NOMA, given that the pilot power-boosting is allowed, can be directly inferred from [7], [8] with the aforementioned assumption of $n_b > 2K$, as follows:

$$C_{\mathrm{LB}} = \left(1 - \frac{K}{n_b}\right) C\left(\gamma_{\mathrm{eff}}\right), \tag{8}$$

where:

$$\gamma_{\mathrm{eff}} = \frac{n_b \mathrm{SNR}}{n_b - 2K} (\sqrt{\alpha} - \sqrt{\alpha - 1})^2 \tag{9}$$

is the *effective* SNR replacing the 'regular' one of eq. (4, 6), and:

$$\alpha = \frac{n_b \mathrm{SNR} + K}{n_b \mathrm{SNR} \frac{n_b - 2K}{n_b - K}}. \tag{10}$$

From eq. (6), the closed-form expression for the lower bound capacity of code-domain NOMA is rewritten as follows:

$$C_{\mathrm{LB}}(\beta, \gamma_{\mathrm{eff}}) = \left(1 - \tfrac{K}{n_b}\right) \sum_{k \geqslant 1} \frac{e^{-\beta} \beta^k}{k!} \int_0^\infty \frac{e^{-\lambda} \lambda^{k-1}}{(k-1)!} \log_2(1 + \gamma_{\mathrm{eff}} \lambda)\, d\lambda, \tag{11}$$

where γ_{eff} is taken from eq. (9).

b) With constraint on pilot power allocation: If the pilot and data symbols are required to have the same power, then solving a convex optimization, depending on SNR, n_b, and K, leads to the following spectral efficiency, in bits/s/Hz [7]:

$$\max_{1 \leqslant n_p \leqslant n_b} \left(1 - \frac{n_p}{n_b}\right) C\left(\frac{\mathrm{SNR}^2 n_p / K}{1 + \mathrm{SNR}(1 + n_p/K)}\right). \tag{12}$$

IV. Results and discussion

In this section, capacity bounds of low-dense NOMA, described in Sec. III, are analyzed as a function of: a) number of coherence symbols n_b; b) number of users K; c) system load $\beta = K/N$. The analysis of lower bound focuses on the case of no pilot power constraint (eq. (11)), the optimal number of pilot symbols, is thus equal to the number of users, i.e. $n_p = K$. An example with pilot power constraint (eq. (12)) is shown for reference in Sec. IV-C.

A. The impact of number of coherence symbols n_b

The calibration of n_b in the 5G context, is particularly relevant for New Radio (5G-NR). According to the duality property from eq. (1), factors that directly affect n_b include the carrier frequency, the symbol period, and vehicular velocities. The new requirements and specifications of 5G has an impact on values of n_b compared to the former generations such as 3GPP LTE [15], or IEEE 802.16 WiMAX [16], in particular:

- The carrier frequency f_c varies within a wide range 1 – 100 GHz, with the deployment of macro sites at lower frequencies, and micro and pico sites at higher frequencies [17].
- Supported mobility speeds v are up to 500 km/h, while the vehicular velocities of interest are about 120 km/h [17].
- According to 3GPP TS 38.211 [5], the most distinguished difference in frame structure of 5G-NR compared to LTE is the so-called numerology, i.e. the subcarrier spacing. In LTE, there is only one type of subcarrier spacing, that is 15 kHz, while multiple types of subcarrier spacing are supported in 5G-NR by scaling up in the power of 2, to the order of fifth numerology, that is, $2^5 \times 15 = 480$ kHz. Since the subcarrier spacing lies between 15 kHz and 480 kHz, its inverse is the symbol period T_s ranging from $2\mu s$ to $66.7\mu s$.

Based on the relationship between n_b and the above parameters, one obtains very high values of n_b if the values of f_c, v, T_s are low and vice versa. Taking into account typical values in the 5G-NR context, n_b can vary from one to thousands, where its range in the earlier generations LTE or WiMAX was only from one to hundreds [8]. This increase is due to the fact that very large spacing of subcarrier in 5G-NR is also supported,

leading to the improvement in the capacity of the pilot-based scheme (c.f. eq. (11)).

Figure 1 shows the capacity bounds of low-dense NOMA as a function of E_b/N_0, with upper bound defined by coherent capacity (solid line) and lower bounds obtained by a pilot-based scheme (via eq.(11)) with fixed $n_p = K = 10$ and different values $n_b = \{25, 50, 100, 500\}$, under the constraint $n_b > 2K$. The system load β is kept fixed and equal to unity, i.e. $K = N$. Although the capacity bounds are considered in the asymptotics, where both K and N should be very large, the order of ten users or REs, however, was mentioned in [4], [18] is enough representative for a large-scale system. Note that, to show a fair comparison among systems, capacity bounds are shown below as a function of E_b/N_0 rather than of SNR via the relation $\frac{E_b}{N_0} = \beta.\text{SNR}/C(\text{SNR})$ [19].

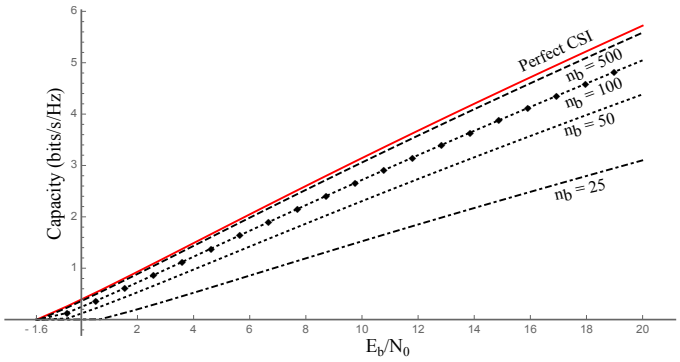

FIGURE 1: Capacity bounds (bits/s/Hz) of low-dense NOMA as a function of E_b/N_0 for fixed $\beta = 1$, with upper bound defined by coherent capacity (solid line) and lower bounds by a pilot-based scheme (eq. (11)) for different values n_b ($n_b = 25, 50, 100, 500$). Note that the pilot power-boosting mode for the pilot scheme is adopted with fixed $n_p = K = 10$.

One may observe that given a same number of users, for e.g. $K = 10$, the scenario producing higher number of symbols in a coherence block benefits the tighter capacity bound to the perfect CSIR case. When n_b is very high and K is fairly low ($n_b = 500, K = 10$), the gap between the upper and lower bounds becomes negligible. Remind that, such a high value of n_b is, in fact, feasible in 5G-NR.

B. The impact of number of users K

The impact of K on the capacity lower bounds of low-dense NOMA, defined by the pilot-based scheme with pilot-boosting power (eq.(11)) is investigated with respect to the number of coherence symbols, for example, up to the favorable value $n_b = 500$. Figure 2 shows capacity lower bounds of low-dense NOMA as a function of n_b with different values $K = \{25, 50, 100\}$, providing fixed $\beta = 1$ and $E_b/N_0 = 10$ [dB]. One may find that the higher the K values, the lower the capacity of the pilot-based scheme, contrarily to MIMO, where the more the transmitting antennas K, the higher the system capacity; in NOMA since the more users, the more pilot symbols, less symbols are available for data transmission. The gap in capacity bounds between the lower $K = 10$ and higher cases $K = 100$ is thus substantial, as shown in Fig. 2.

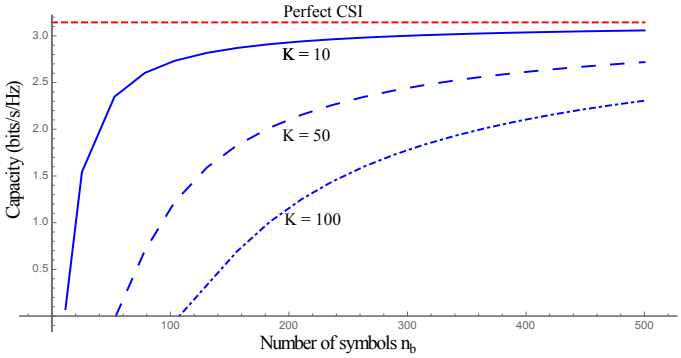

FIGURE 2: Capacity lower bounds (bits/s/Hz) of low-dense NOMA pilot-based scheme (eq.(11)) with fixed $n_b = 500$, $\beta = 1$ and $E_b/N_0 = 10$ [dB] as a function of n_b with different values $K = \{10, 50, 100\}$.

C. The impact of system load β

The system load $\beta = K/N$, which is an important factor in code-domain NOMA [4], leads to underloaded and overloaded systems when the number of users K is lower (or $\beta < 1$) or higher than the number of REs (or $\beta > 1$). For optimum receivers, it was shown in [4], [12], [19] that the coherent capacity and the capacity lower bounds increase along with system load, irrespective of dense vs. low-dense spreading formats. Figure 3 displays the coherent capacity and its lower bounds given for the pilot-boosting power case as a function of β for fixed $E_b/N_0 = 10$ [dB] in different n_b and K combinations, such as $\{n_b, K\} = \{25, 10\}, \{100, 10\}, \{500, 10\}, \{500, 100\}$. When β increases, the capacity lower bounds with more coherence symbols (high n_b) and few users (low K) reach closer to the upper bound, as also observed in the $\beta = 1$ case. It is worthy to note that, the same lower capacity bounds can be attained given the same scaling of the combination $\{n_b, K\}$.

The capacity lower bound with the power constraint mode for the case $\{n_b = 25, K = 10\}$ is also shown in Fig. 3, and is, as expected, lower than that of without pilot power constraint, given the same combination $\{n_b, K\}$. From $\beta > 1$, the gap among the different cases expands substantially, particularly the lower bound derived for the case with pilot power constraint.

V. CONCLUSION

Information-theoretical bounds of low-dense code-domain NOMA, under the hypothesis of Rayleigh block-fading channels without CSI, were derived. The capacity upper bound, defined as the capacity of low-dense NOMA with perfect CSI, was found based on the general framework proposed in [4]. The capacity lower bound was derived using a pilot-based communication scheme, as suggested in [7]. Upper and lower capacity bounds were described as a function of E_b/N_0, number of coherent symbols n_b, and system load β. The effect of the number of users K was also investigated. Results

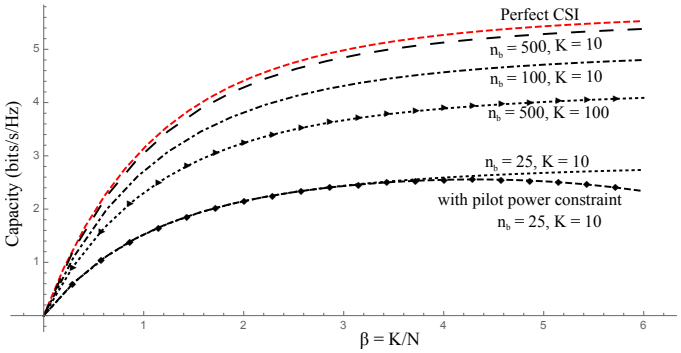

FIGURE 3: Capacity bounds of low-dense code-domain NOMA scheme with upper bound being the coherent capacity and lower bound obtained with a pilot-based scheme as a function of $\beta = K/N$ and fixed $E_b/N_0 = 10$ [dB].

indicate that, when the above factors are favourably combined, the gap between the upper and lower capacity bounds becomes negligible. In particular, when the number of symbols n_b is high, while the number of users simultaneously joining the network is low, the lower capacity bound well approximates the capacity with perfect CSI, leading to the conclusion that the system is robust despite the absence of knowledge on the channel.

REFERENCES

[1] G. Durisi, U. G. Schuster, H. Bölcskei, and S. Shamai, "Noncoherent capacity of underspread fading channels," *IEEE Trans. Inf. Theory*, vol. 56, no. 1, pp. 367–395, Jan. 2010.

[2] L. Zheng and D. N. Tse, "Communication on the Grassmann manifold: A geometric approach to the noncoherent multiple-antenna channel," *IEEE Trans. Inf. Theory*, vol. 48, no. 2, pp. 359–383, Feb. 2002.

[3] L. Dai, B. Wang, Y. Yuan, S. Han, C. l. I, and Z. Wang, "Non-orthogonal multiple access for 5G: solutions, challenges, opportunities, and future research trends," *IEEE J. Sel. Areas Commun.*, vol. 53, no. 9, pp. 74–81, Sept. 2015.

[4] M. T. P. Le, G. C. Ferrante, T. Q. S. Quek, and M.-G. Di Benedetto, "Fundamental Limits of Low-Density Spreading NOMA with Fading," *IEEE Trans. Wireless Commun.*, 2018, to be appeared.

[5] 3rd Generation Partnership Project (3GPP), *TS 38.211. NR; Physical channels and modulation*, 2017, [Online]. Available: http://www.3gpp.org/ftp/Specs/html-info/38211.htm.

[6] M. Médard, "The effect upon channel capacity in wireless communications of perfect and imperfect knowledge of the channel," *IEEE Trans. Inf. Theory*, vol. 46, no. 3, pp. 933–946, May 2000.

[7] B. Hassibi and B. M. Hochwald, "How much training is needed in multiple-antenna wireless links?" *IEEE Trans. Inf. Theory*, vol. 49, no. 4, pp. 951–963, Apr. 2003.

[8] F. Rusek, A. Lozano, and N. Jindal, "Mutual information of IID complex gaussian signals on block rayleigh-faded channels," *IEEE Trans. Inf. Theory*, vol. 58, no. 1, pp. 331–340, Jan. 2012.

[9] N. Jindal and A. Lozano, "A unified treatment of optimum pilot overhead in multipath fading channels," *IEEE Trans. Commun.*, vol. 58, no. 10, pp. 2939–2948, Oct. 2010.

[10] S. Shamai and S. Verdú, "The impact of frequency-flat fading on the spectral efficiency of CDMA," *IEEE Trans. Inf. Theory*, vol. 47, no. 4, pp. 1302–1327, May 2001.

[11] A. M. Tulino and S. Verdú, "Random matrix theory and wireless communications," *Foundations and Trends in Commun. and Inf. Theory*, vol. 1, no. 1, pp. 1–182, 2004.

[12] G. C. Ferrante and M.-G. Di Benedetto, "Spectral efficiency of random time-hopping CDMA," *IEEE Trans. Inf. Theory*, vol. 61, no. 12, pp. 6643–6662, Dec. 2015.

[13] E. Telatar, "Capacity of Multi-antenna Gaussian Channels," *Transactions on Emerging Telecommunications Technologies*, vol. 10, no. 6, pp. 585–595, 1999.

[14] T. L. Marzetta, "BLAST training: Estimating channel characteristics for high capacity space-time wireless," in *Proc. Allerton Conf. on Commun., Control, and Computing (Allerton)*, vol. 37, 1999, pp. 958–966.

[15] *UTRA-UTRAN Long Term Evolution (LTE)*. 3rd Generation Partnership Project (3GPP), Nov. 2004.

[16] J. G. Andrews, *Fundamentals of WiMAX: Understanding Broadband Wireless Networking*. Prentice Hall PTR, Nov. 2007.

[17] K. Haneda *et al.*, "Indoor 5G 3GPP-like channel models for office and shopping mall environments," in *Proc. IEEE Int. Conf. Commun. (ICC)*, May 2016, pp. 694–699.

[18] D. Guo and S. Verdú, "Randomly Spread CDMA: Asymptotics via Statistical Physics," *IEEE Trans. Inf. Theory*, vol. 51, no. 6, pp. 1983–2010, June 2005.

[19] S. Verdú and S. Shamai, "Spectral efficiency of CDMA with random spreading," *IEEE Trans. Inf. Theory*, vol. 45, no. 2, pp. 622–640, Mar. 1999.